Construction and Building Materials 170 (2018) 649–659

Contents lists available at ScienceDirect

Construction and Building Materials

journal homepage: www.elsevier.com/locate/conbuildmat

Effect of coarse basalt aggregates on the properties of Ultra-high Performance Concrete (UHPC)

P.P. Li [a,b], Q.L. Yu [b,*], H.J.H. Brouwers [a,b]

[a] State Key Laboratory of Silicate Materials for Architectures, Wuhan University of Technology, Wuhan 430070, PR China
[b] Department of the Built Environment, Eindhoven University of Technology, P.O. Box 513, 5600 MB Eindhoven, The Netherlands

HIGHLIGHTS

- UHPC incorporating coarse basalt aggregate is designed.
- The mineral admixture effect on fluidity, strength and drying shrinkage of UHPC pastes is assessed.
- The basalt aggregate size effect on the strength of UHPC is studied.
- The powder content effect on compactness, strength and distribution modulus of UHPC is analysed.
- The interaction between coarse aggregate and steel fibre in UHPC is discussed.

ARTICLE INFO

Article history:
Received 25 October 2017
Received in revised form 9 March 2018
Accepted 13 March 2018

Keywords:
Ultra-high Performance Concrete
Coarse aggregate
Mineral admixture
Powder content
Compactness
Distribution modulus
Steel fibre

ABSTRACT

In the present research, Ultra-high Performance Concretes (UHPCs) applying coarse basalt aggregate with a maximum particle size of 16 mm are designed by using the particle packing theory and considering optimal powder proportion. The fluidity, shrinkage, strength of paste, and the compressive and tensile splitting strength of UHPC are investigated. The effect of coarse basalt aggregate size and resulting powder content change are evaluated. Furthermore, the mineral admixture effect, interaction between aggregate and steel fibre are analysed and discussed. The results show that the optimal proportion of powder is 5% of micro-silica and 20% of limestone powder by mass of the total powder. The coarse basalt aggregate has limited reducing effect on the mechanical strength of UHPC. The optimal powder content of about 800 kg/m^3 and 700 kg/m^3 is found for UHPC when the maximum basalt aggregate size is 8 mm and 16 mm, respectively. Furthermore, a distribution modulus q of 0.19 for the modified Andreasen and Andersen model is recommended for designing UHPC with coarse aggregates. The optimal powder contents are the same for UHPC without and with 2 vol% steel fibre, and longer fibre is suggested for UHPC with coarser aggregate.

1. Introduction

Ultra-high Performance Concrete (UHPC) is a relatively new building material, which has superior mechanical strength, ductility, impact resistance, fatigue resistance and durability [1–5]. The UHPC usually can be designed with various cementitious components, fine or ultra-fine aggregates, high strength fibres, chemical admixtures and water. The performance of UHPC is greatly dependent on the type, size and proportion of those raw materials [6]. To obtain an excellent mix design of UHPC, it is important to understand the effect and mechanism of those ingredients on the properties of UHPC.

To avoid the limit of intrinsic strength of coarse aggregate, overcome the inherent weakness between coarse aggregate and paste matrix, increase the homogeneity and eliminate stress concentration at the contact points between those aggregates, most of UHPCs are designed by using only fine aggregates or refined aggregate [1–3]. However, concrete containing appropriate type and content of coarse aggregate can possess certain advantages. Rozalija and Darwin [7] reported that high-strength concrete containing basalt aggregate yields higher mechanical properties than high-strength concrete containing limestone, which is attributed by the intrinsic strength of the rock. Ma et al. [8] reported that coarse aggregate can improve the elastic modulus and alter the workability of UHPC more easily, as well as reduce the cost. Some researchers presented that an addition of coarse aggregate does not reduce or even exhibits a slightly higher compressive strength [9,10]. With

* Corresponding author.
E-mail address: q.yu@bwk.tue.nl (Q.L. Yu).

https://doi.org/10.1016/j.conbuildmat.2018.03.109
0950-0618/

the utilization of coarse aggregate, the autogenous shrinkage was reduced by approximately 40% [2]. Peng et al. [11] suggested to use coarse basalt aggregate to improve the penetration impact resistance. Tai et al. [12] presented that at higher loading rates (impact loading), the cracks form quickly and can propagate through the aggregates, consequently increasing the impact resistance. Both the disadvantages and advantages are very considerable for concrete incorporating coarse aggregate. To utilize the coarse aggregate in UHPC, these contradictions should be well balanced. Hence, it is of importance to study the aggregate size effect in UHPC. In this study, basalt aggregates are used to match the high strength of paste matrix of UHPC.

Currently, most UHPCs are designed with a high content of powder, which leads to poor economic benefit and low efficiency [13]. On the other hand, a relatively high content of powder is needed to fill the voids between the aggregates to reduce the contact stress concentration and result in a homogenous stress distribution through the matrix [14]. Normally, the powder volume fraction in UHPC containing coarse aggregate is lower than that without coarse aggregate [8]. Some investigations show that the compressive strength of self-compacting concrete (SCC) increases noticeably with the increase of powder content, especially in lower water-to-cement ratios [15]. But Domone [16] pointed out that there was no discernible trend of variation on the mechanical properties of SCC when increasing the powder contents. Therefore, it is necessary to further understand the powder content effect and find an optimal amount for UHPC when coarse basalt aggregates are utilized. Steel fibre is a critical ingredient because of its considerable reinforcement on mechanical properties, especially for tensile strength, ductility and energy dissipation. The interaction effect between coarse aggregate and steel fibre is also researched on the UHPCs with different powder contents in the present study, as well as the discussion of fibre length for UHPC with coarser aggregate.

The powder content in an UHPC matrix will be consequently altered when applying coarse aggregate with different sizes. Various cementitious materials have been utilized to produce UHPC, such as Portland cement, micro-silica, slag, fly ash, metakaolin, limestone powder, nanoparticles, etc. As an industrial by-product from the exhaust gases of ferrosilicon, silicon, and other metal alloy smelting furnaces, micro-silica is an essential constituent for UHPC. Previous researches have already shown that micro-silica can improve the microstructure of UHPC by pozzolanic, filling and nucleation effects, consequently improving its strength, interfacial transition zone (ITZ), durability, etc. [17–20]. Amorphous SiO_2 in micro-silica can react with $Ca(OH)_2$ from the hydration of cement to produce C-S-H. The ultra-fine particle in micro-silica can provide nucleation site to accelerate the cement hydration, as well as act as good filler. As a non-pozzolanic mineral admixture, the limestone powder is mainly used as a filler to partially replace cement. Recent researches indicate that the particle surface of limestone powder is an active template for the nucleation and growth of cement hydration products [21]. Somewhat soluble limestone powder contributes to preferably form the carboaluminate hydration instead of monosulfate [21,22]. It can improve the fluidity and microstructure of concrete, and has a positive effect on the generation of C-S-H gel [23,24]. However, there are still some problems for utilizing micro-silica and limestone powder in UHPC. Too much micro-silica can lead to poor fluidity [25] due to the high water demand and agglomeration [26,27] due to the high surface energy, especially for UHPC with low water-to-powder ratio. Too high content of limestone powder can result in the decrease of the mechanical strength due to the dilution effect on binders. Furthermore, the optimal contents of those mineral admixtures are highly dependent on the water-to-cement ratio [19], which indicates the optimal amount in normal concrete is not suitable to UHPC with relatively low water content. Therefore, investigating the optimal contents of micro-silica and limestone powder in UHPC is still a challenging issue. It is of great significance to investigate the mineralogical composition and understand the synergetic effects of those different powders for properly designing the UHPC.

The objective of this study is to investigate the effect of coarse aggregate size and the consequent alteration of powder content on the properties of UHPC. In addition, the mineral admixture effect, and interaction between basalt aggregate and steel fibre are investigated. The optimum content of micro-silica and limestone powder is attained, based on the workability, mechanical strength and shrinkage of paste. Then, UHPCs applying coarse basalt aggregate are designed by using the particle packing theory and optimal mineral proportion. The basalt aggregate size effect on mechanical strength is measured and analysed. The powder content effect on compactness and strength of UHPC with coarse basalt aggregate is analysed and discussed, and optimum powder content and corresponding value of distribution modulus q are suggested. The strength improvement of UHPC is measured with 2 vol% steel fibre, and interaction between coarse basalt aggregate and steel fibre is discussed.

2. Experimental program

2.1. Materials

The raw materials used in this study are Portland Cement CEM I 52.5 R (CEM), micro-silica (mS), limestone powder (LP), sand 0–2 (S), basalts aggregate (BA), water (W), PCE-type superplasticizer (SP). The steel fibre (SF) (length = 13 mm, diameter = 0.2 mm, tensile strength = 1100 MPa) is utilized to investigate the reinforcement ratio for UHPC under different powder contents. The dosage of steel fibre is 2% vol. of the UHPC, which is proven to be an appropriate dosage for UHPC [3,28]. The specific densities of those ingredients are measured by a gas pycnometer (AccuPyc 1340 II Pycnometer), shown in Table 1. The particle size distributions (PSD) of the used materials are measured by the sieve and laser diffraction analyses (Malvern Mastersizer 2000®), respectively, shown in Fig. 1. The particle morphologies of the used powders are tested by scanning electron microscopy (SEM, Phenom ProX), shown in Fig. 2. The chemical compositions of the used powders are tested by X-ray Fluorescence (XRF), shown in Table 2.

2.2. Mix design of mixtures

To study the mineral admixture effect and obtain optimal proportions of all powders (CEM, mS, LP), the pastes (containing powder, water and SP) were designed with a water-to-powder ratio (w/p) of 0.2 and SP dosage of 0.8% by the weight of total powder. The mS and LP were changed from 5% to 15%, 10% to 30% by the weight of total powder, respectively. To further study the mechanism of different mineral admixtures on the fluidity, the water demand of the individual powder is determined by the mini spread flow test.

The recipes of UHPCs are shown in Table 3. The mS and LP are fixed at 5% and 20% by mass of total powder, respectively, based on the investigation of the mineral admixture effect. To research the effect of basalt aggregate size on the strength of UHPC, the powder content of UHPC is fixed at 900 kg/m^3, considering that most UHPC incorporates powder more than 900 kg/m^3 [4,19,29–33]. To investigate the effect of powder content on the compactness and strength of UHPC, the powder contents are changed from 900 kg/m^3 to 650 kg/m^3. The fraction of the basalt aggregates are

Table 1
Specific densities of raw materials.

Materials	CEM	mS	LP	S	BA 8-11	BA others	W	SP	SF
Specific density (g/cm^3)	3.15	2.32	2.71	2.72	2.89	3.05	1.00	1.07	7.85

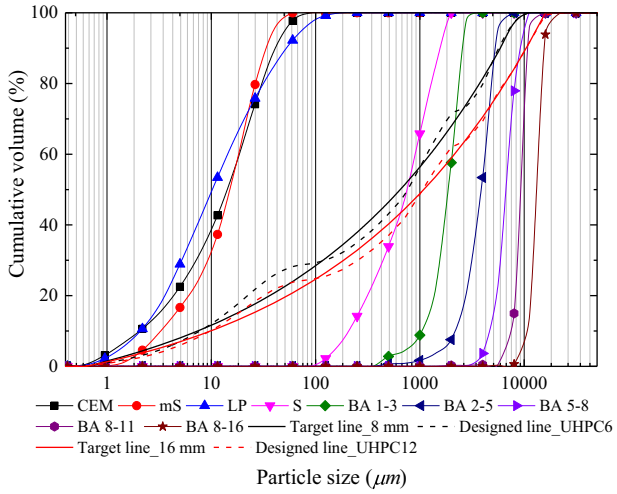

Fig. 1. The PSDs of raw materials and UHPCs.

calculated by using the modified Andreasen and Andersen model as follows [34–38]:

$$P(D) = \frac{D^q - D_{min}^q}{D_{max}^q - D_{min}^q} \quad (1)$$

$$RSS = \sum_{i=1}^{n} \left[P_{mix}\left(D_i^{i+1}\right) - P_{tar}\left(D_i^{i+1}\right) \right]^2 \rightarrow min \quad (2)$$

in which D is the particle size, D_{min} and D_{max} represent the minimum and maximum particle size, respectively; $P(D)$ is the cumulative fraction of the total solids being smaller than size D; q is the distribution modulus, and 0.22 is used in this study as recommended in [39,40], P_{mix} is the designed mix, and the P_{tar} is the target grading calculated from Eq. (1). The proportions of each basalt aggregate in the designed mixture are adjusted until an optimum fit between P_{mix} (D) and P_{tar} (D), using an optimization algorithm based on the Least Squares Method, as presented in Eq. (2). It should be pointed out that the 750 kg/m^3 and 650 kg/m^3 are the optimum powder content for the UHPC with the maximum aggregate size of 8 mm and 16 mm, respectively, based on the modified Andreasen and Andersen model without any fixed condition of powder content. Examples of the PSDs of the target and designed curve of UHPCs are shown in Fig. 1.

To research the interaction between coarse aggregate and steel fibre, Ultra-high Performance Fibre Reinforced Concretes (UHPFRCs) were designed, based on the designed UHPCs (in Table 3) with reinforcement of 2 vol% steel fibre.

2.3. Mixing regimes for mixtures

The mixing of mixtures lasts about 5.5 min (paste), 8 min (UHPC) and 10 min (UHPFRC), respectively, by using a 20-liter Hobart mixer. The dry mixing of powders and sand is conducted for about 1 min, sequentially adding 75% water, mixed solution of 25% water and superplasticizer product, steel fibre and basalt aggregate. The detailed mixing regimes are shown in Fig. 3.

2.4. Testing methods

2.4.1. Fresh behaviour

The spread flow of pastes was measured by using a truncated conical mould (Hägermann cone: height 60 mm, top diameter 70 mm, bottom diameter 100 mm), in accordance with EN 1015-3 [41]. Fresh paste was filled in the mould and the cone was lifted straight upwards to allow the paste flow freely without jolting. The spread flow was calculated by the average value of two perpendicular diameters. The flow tests were conducted at room temperature of about 20 ± 1 °C.

The water demand of powder is greatly influenced by a layer of adsorbed water around the particles and inter-granular water, which can strongly affect the fresh behaviour of concrete, especially for UHPC with low water-to-powder ratio. In this study, the water demands of powders are evaluated by the relative slump method, a detailed information about the method can be found in [35,36,42,43]. The relative slump is calculated by using the mini-spread flow, as shown above. Several mixes with different water-to-powder ratios were measured in order to obtain a statistically reliable trend line for the regression analysis.

2.4.2. Mechanical strength

The fresh pastes were casted into plastic moulds (40 × 40 × 160 mm^3) and steel cubic moulds (100 × 100 × 100 mm^3) for flexural and compressive strength tests, respectively. The fresh UHPCs

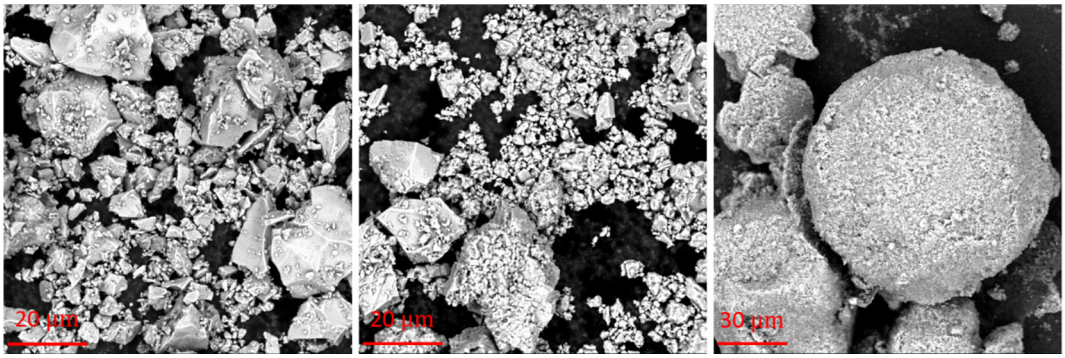

Fig. 2. Particle morphologies of (a) CEM, (b) LP, (c) mS by SEM.

Table 2
Chemical composition of powders.

Substance (%)	CaO	SiO_2	Al_2O_3	Fe_2O_3	K_2O	Na_2O	SO_3	MgO	TiO_2	MnO
CEM	64.60	20.08	4.98	3.24	0.53	0.27	3.13	1.98	0.30	0.10
mS	0.90	93.06	–	2.06	1.15	0.63	1.28	0.70	–	0.07
LP	97.21	0.87	0.17	0.13	–	–	0.11	1.17	0.01	0.01

Table 3
Recipes of UHPCs with different basalt sizes and powder contents (kg/m^3).

No.	Note a-b	CEM	mS	LP	S	BA 1-3	BA 2-5	BA 5-8	BA 8-11	BA 8-16	W	SP
UHPC1	3-900	675.0	45.0	180.0	864.5	576.3	0	0	0	0	180.0	10.8
UHPC2	8-900	675.0	45.0	180.0	588.1	178.6	403.1	313.9	0	0	180.0	10.8
UHPC3	16-900	675.0	45.0	180.0	304.7	308.3	306.6	247.5	120.9	206.2	180.0	10.8
UHPC4	8-850	637.5	42.5	170.0	700.1	100.5	435.7	310.4	0	0	170.0	10.2
UHPC5	8-800	600.0	40.0	160.0	812.2	22.3	468.4	307.0	0	0	160.0	9.6
UHPC6	8-750	562.5	37.5	150.0	903.6	0	318.8	453.8	0	0	150.0	9.0
UHPC7	16-900	675.0	45.0	180.0	242.9	338.9	278.6	251.5	109.9	200.7	207.0	5.4
UHPC8	16-850	637.5	42.5	170.0	355.0	259.4	315.4	238.5	118.1	203.1	195.5	5.1
UHPC9	16-800	600.0	40.0	160.0	467.2	179.9	352.2	225.3	126.4	205.4	184.0	4.8
UHPC10	16-750	562.5	37.5	150.0	579.3	100.4	389.0	212.2	134.6	207.8	172.5	5.3
UHPC11	16-700	525.0	35.0	140.0	698.7	0.6	445.2	186.9	147.8	209.6	161.0	4.9
UHPC12	16-650	487.5	32.5	130.0	782.6	0.0	406.6	221.5	136.2	213.9	149.5	4.6

a and b means the maximum particle size of used basalt and powder content, respectively. The water-to-powder ratio of No. UHPC1 – UHPC6 is fixed at 0.2, while the water-to-powder ratio of No. UHPC7 – UHPC12 is fixed at 0.23.

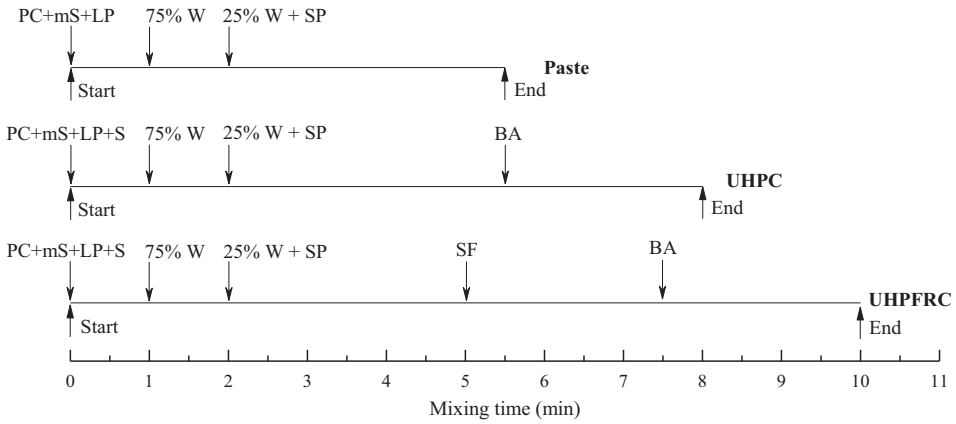

Fig. 3. Mixing regimes for mixtures.

were casted into steel cubic moulds ($100 \times 100 \times 100\ mm^3$). All samples were covered with polyethylene film to prevent the moisture loss. They were demoulded approximately 24 h after casting and then cured in water under room temperature of 20 ± 1 °C. The compressive and flexural strength of paste samples were tested after 7 days and 28 days, based on EN 12390-3 [44] and EN 196-1 [45], respectively. The compressive and tensile splitting strength of UHPC samples were measured after 28 days, based on EN 12390-3 [44] and EN 12390-6 [46].

2.4.3. Shrinkage

The fresh pastes were casted into $40 \times 40 \times 160\ mm^3$ moulds for shrinkage test based on DIN 52450-A [47], then covered by a polyethylene film and cured at room temperature of 20 ± 1 °C. The samples were demoulded after 24 h and then cured in an environmental chamber (50% RH, 20 ± 1 °C). The initial length along the longitudinal axis of sample was measured by adopting a digital length comparator (±0.001 mm) immediately after demoulding. The changed length was recorded at desired ages within 91 days.

3. Results and discussion

3.1. Mineral admixture effect

3.1.1. Water demand of powder

The water demand of powder is greatly dependent on its physical and chemical characteristics, which subsequently influence the flowability. To investigate the water demand of different powders, the relative slump Γ_p was calculated [35,48]:

$$\Gamma_p = \left(\frac{d}{d_0}\right)^2 - 1; \quad d = \frac{d_1 + d_2}{2} \tag{3}$$

where d_1 and d_2 are the perpendicular diameters of the spread flow, d_0 is the cone base diameter (100 mm). The relative slump can be plotted versus w/p and a linear trend line can be plotted thus [36,42]:

$$\frac{V_w}{V_p} = \beta_p + E_p\Gamma_p \tag{4}$$

where V_w and V_p represent the volume of water and powder. β_p is as water demand and represents the minimum water content to assure a fluid paste. The deformation coefficient (E_p) is derived from the slope of the linear regression line, which indicates the sensitivity of the materials on the water demand for a specified workability. To intuitively understand the replacement effect of different powders on flowability by mass, the linear relation between water-to-powder ratio and relative slump is proposed as:

$$\frac{m_w}{m_p} = \beta'_p + E'_p \Gamma_p \tag{5}$$

where m_w and m_p are the mass of water and powder. $\beta'_p = \rho_w/\rho_p \beta_p$ and $E'_p = \rho_w/\rho_p E_p$ are the water demand and deformation coefficient expressed by mass. ρ_w and ρ_p are the specific density of water and powder, respectively.

Domone and His-wen [49] experimentally proved that it is possible to estimate values of β_p and E_p for powder mixtures by a simple law of mixtures (namely, from those for the individual powders). The water demand and deformation coefficient can be expressed as:

$$\beta_p = \sum_{i=1}^{n} \frac{V_{pi}}{V_p} \beta_{pi}; E_p = \sum_{i=1}^{n} \frac{V_{pi}}{V_p} E_{pi} \tag{6}$$

where i represents the type number of different powders. According to the Eqs. (4)–(6), the water-to-powder ratio can be derived as follows:

$$\frac{m_w}{m_p} = \frac{\rho_w V_w}{\rho_p V_p} = \sum_{i=1}^{n} \frac{m_{pi}}{m_p} \beta'_{pi} + \sum_{i=1}^{n} \frac{m_{pi}}{m_p} E'_{pi} \Gamma_p \tag{7}$$

Eqs. (5) and (7) indicate that β'_p and E'_p for powder mixtures also comply with a simple law of mixtures, as follows:

$$\beta'_p = \sum_{i=1}^{n} \frac{m_i}{m_p} \beta'_{pi}; E'_p = \sum_{i=1}^{n} \frac{m_i}{m_p} E'_{pi} \tag{8}$$

Hence, it is reasonable to use the water demand of individual powder by mass to explain the replacement effect of mineral admixtures on the flowability of paste.

Fig. 4 shows that water demand of different powders by mass proportion. The largest water demand (β'_p) can be observed for micro-silica of 0.48, followed by cement of 0.39 and limestone powder of 0.31. It indicates that the substitution of cement by limestone powder can increase the flowability, while addition of micro-silica results in reduced fluidity. Fig. 4 also shows smaller deformation coefficients (E'_p) of micro-silica and limestone powder than that of cement, which indicates that those two materials are more sensitive to water amount than the cement. Therefore, the blended paste is more sensitive to water addition than plain cement paste.

3.1.2. Flowability of paste

Fig. 5 shows the spread flow of pastes incorporating different contents of micro-silica and limestone powder. With the increase of micro-silica content, the spread flow decreases continuously because of the much larger water demand of micro-silica than that of cement. The maximum decrease occurs at the limestone powder content of 10%, from 29 mm to 11.4 mm. The reason is that the micro-silica with very fine particle sizes adsorbs much superplasticizer on the surface [50] and decreases the amount of lubricating water available within the inter particle voids [43]. Furthermore, micro-silica has a high reactivity due to its fineness and pozzolanic property, which increase the inter-particles friction [26]. The increasing addition of limestone powder improves the fluidity greatly, especially at the micro-silica content of 15%, which increases from 11.4 mm to 27.4 mm. The limestone powder has a neutral surface with the main constituent of Ca^{2+} and CO_3^{2-} ions. The groups of OH^- localize over the Ca^{2+} surface in aqueous solution, leading to inter-particle electrostatic repulsion, which consequently reduces cement particle flocculation and enhances the flowability of the paste [21,51]. Furthermore, the less water demand of limestone powder than that of cement (seen in Fig. 4) contributes to improved fluidity of cementitious pastes. The spread flow can be classified into 6 levels (in Fig. 5). With the linearly increasing content of micro-silica from 5% to 10%, the content of limestone powder should be almost linearly increased from 20% to 30%, to attain the first level (35–40 mm).

3.1.3. Mechanical strength of paste

The flexural and compressive strengths of pastes are depicted in Figs. 6 and 7. A relatively low content of micro-silica and limestone powder tends to improve both flexural and compressive strength, especially for the 7 days strength. A too high content (more than 5%) of micro-silica results in negative effect on the strength, attributed to dispersion problems and agglomeration of particles, which is similar to nano-silica [26,52]. A higher content (more than 20%) of limestone powder decreases the strength of paste because of dilution effect due to the cement reduction, resulting in less hydra-

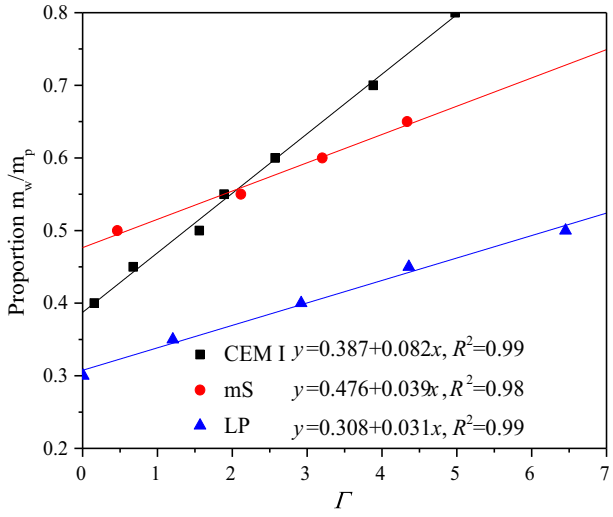

Fig. 4. Water demand of different powders.

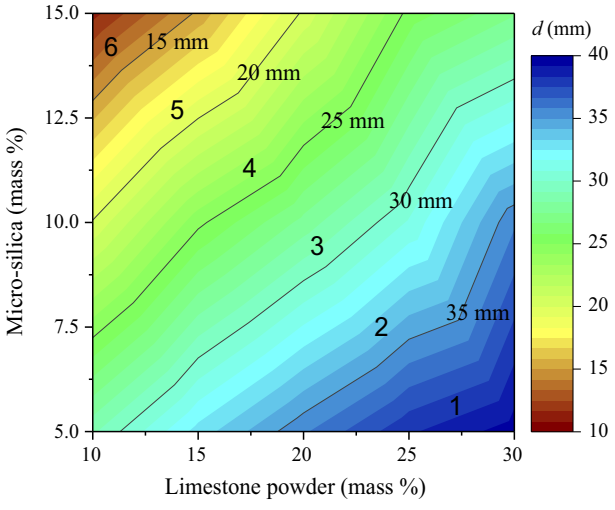

Fig. 5. Spread flow of pastes.

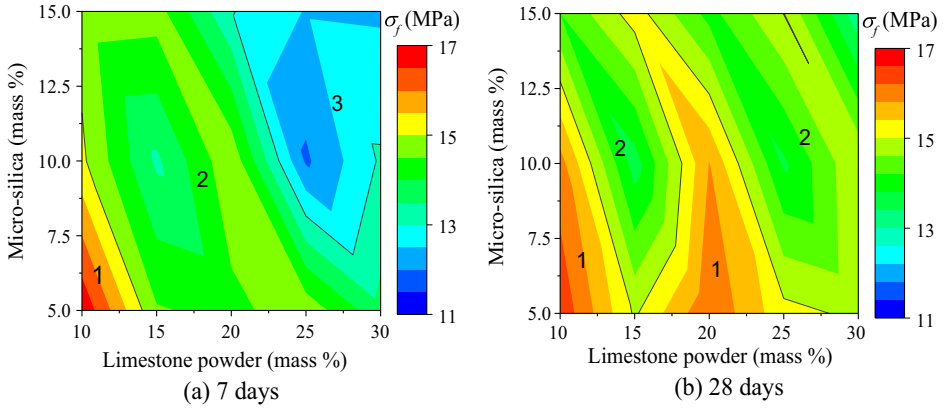

Fig. 6. Flexural strength of pastes at (a) 7 days and (b) 28 days.

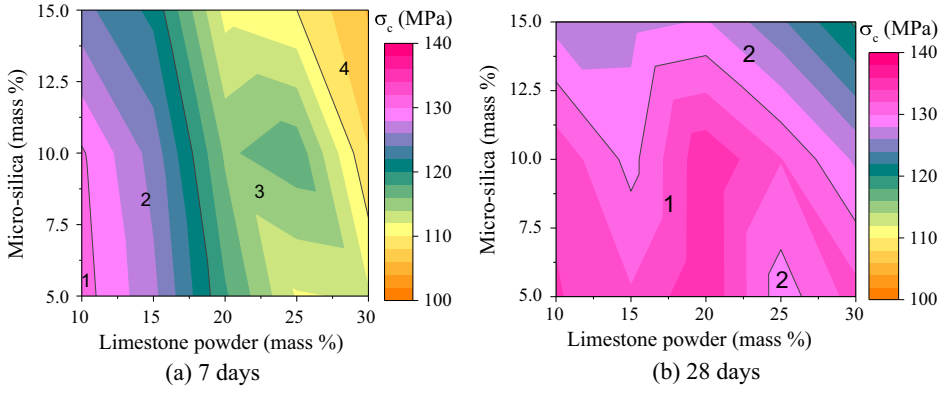

Fig. 7. Compressive strength of pastes at (a) 7 days and (b) 28 days.

tion products and weaker bonding force. However, it is important to notice that the 28 days strength of pastes are only slightly reduced or even slightly improved at a higher content of micro-silica and limestone powder, which is in line with [53]. The pozzolanic reaction of micro-silica with calcium hydroxide forms more C-S-H gel and fills the remaining voids at later stages, which refines the microstructure and improves mechanical properties [36]. Furthermore, somewhat soluble limestone powder contributes to preferably forming the carboaluminate instead of monosulfate [21,22]. The carboaluminate is stiffer than conventional cement hydration products and increases mechanical properties. An appropriate limestone powder amount causes a nucleation effect which accelerates the hydration reaction and causes more C-S-H gel [23,24] and improves the microstructure.

The compressive strength of pastes with micro-silica less than 5% is also measured to find the optimum content of micro-silica, as shown in Fig. 8. To summarize, the optimal proportion of powders is 5% of micro-silica and 20% of limestone powder by mass of total powder by considering both fluidity and strength of pastes, which will be used in the following mix design of UHPCs. Vance et al. [54] modified the hydration and strength development of Portland cement with ternary blends containing 10% limestone and 10% fly ash or metakaolin. Wang et al. [55] also successfully introduced 20% to UHPC containing 10% mS and 20% ground granulated blastfurnace slag.

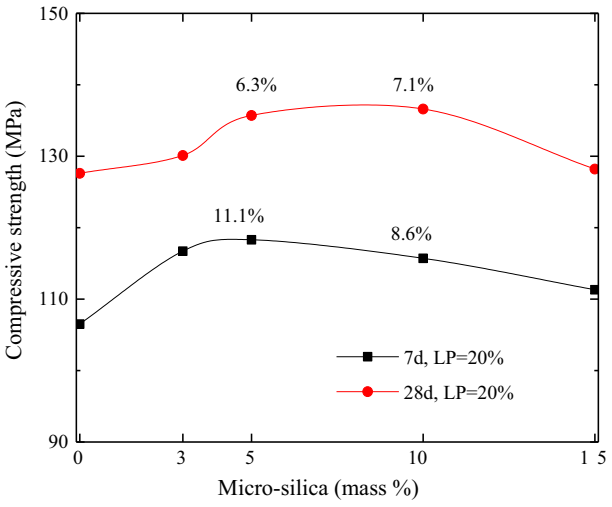

Fig. 8. Compressive strength of pastes (LP = 20%).

3.1.4. Shrinkage of paste

Some researchers have already indicated that mineral admixtures affect the shrinkage behaviour of concrete significantly [56–60]. But the relevant research is very limited in UHPC with relatively low water amount. According to the Mackenzie equation [61], the shrinkage strain can be expressed as:

$$\varepsilon_p = \sigma_{cap}\left(\frac{1}{3K} - \frac{1}{K_s}\right) \tag{9}$$

where K is bulk modulus of the whole porous body and K_s is bulk modulus of the solid material. The capillary tensile stress can be calculated according to the Kelvin-Laplace equation [62]:

$$\sigma_{cap} = \frac{2\gamma cos\alpha}{r} = \frac{-\ln(RH)\rho RT}{M} \quad (10)$$

where M is molar weight of water, ρ is density of water, R is ideal gas constant, RH is the relative humidity and T is absolute temperature. It can be seen that the mineral admixture effect on shrinkage is greatly dependent on the different abilities of capillary water loss in different cementitious systems.

The shrinkages of pastes incorporating different contents of micro-silica and limestone powder are shown in Fig. 9. Within 91 days, the mixture with a mass replacement of cement by 5% micro-silica shows a similar behaviour in shrinkage strain to plain cement paste, which is probably due to the mutual effects of higher reactivity (positive) and better pore structure refinement (negative) by C-S-H gel formed [63]. While, substitution of cement by 20% limestone powder shows a considerable increase of absolute value of shrinkage, up to 1.6 times after 91 days compared to the plain cement paste. However, Itim et al. [53] found that 25% addition of limestone powder generates a similar total shrinkage to that of ordinary Portland cement after half year, while Benachour et al. [64] reported the addition can even be up to 35%. The considerably different effect of limestone powder on the shrinkage is attributed to the relatively low water-to-powder ratio in the present case. With the partial substitution by limestone powder for a low amount, the relative water-to-binder ratio increases greatly, consequently increasing the porosity (especially for small pores), which makes the relative humidity (RH) loss more easily in Eq. (10) and enlarges shrinkage of the paste. Furthermore, the dilution effect by limestone powder contributes to low reactivity and leaves more free water in the pore structure. The loss of those free water can increase the capillary tensile stress and enlarge the shrinkage. In the presence of 20% limestone powder, 5% micro-silica can greatly inhibit the shrinkage, approximately 15% reduction. The micro-silica in paste can reduce the small capillary pores of the paste matrix due to formation of more C-S-H gel by pozzolanic reaction with calcium hydroxide, subsequently reduces the diffusion of the capillary and adsorbed water to the environment, which is the main cause of the shrinkage mechanism [65].

In a short summary, limestone powder has the lowest water demand, and an excellent fluidity can be obtained with substitution of cement by 20% limestone powder, without sacrifice of mechanical strength. However, 20% limestone powder replacement enlarges the shrinkage greatly, while 5% micro-silica addition is observed to greatly inhibit the shrinkage in the presence of 20% limestone powder. Nevertheless, higher micro-silica dosage is not preferred as it will lead to dramatic reduction on workability and increase on cost. Hence, by considering the properties of water demand, flowability, mechanical strength and shrinkage, the optimal proportion of 5% micro-silica and 20% limestone powder by mass of total powder is recommended, which is used as a fixed composition in the following investigations in this study.

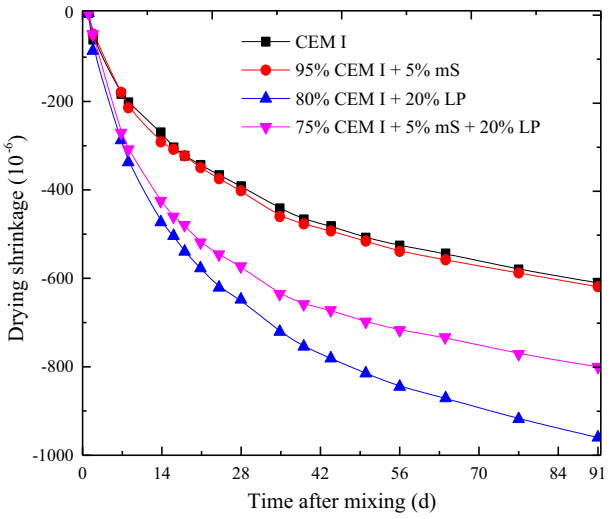

Fig. 9. Shrinkage of pastes.

3.2. Basalt aggregate size effect

Fig. 10 presents the compressive and tensile splitting strength of UHPCs versus the maximum size of basalt after 7 days and 28 days, respectively. The results show that the 7 days compressive strength of UHPCs do not have obvious difference, namely at about of 122 MPa, while the tensile splitting strength of UHPCs has a linear decrease from 9.1 MPa to 6.1 MPa. At 28 days, the compressive strength has a linear decrease trend from 144 MPa to 132 MPa, while the tensile splitting strength shows a slight decrease from 9.8 MPa to 8.2 MPa, with the maximum basalt size changing from 3 mm to 16 mm.

The decrease tendency of strength caused by the larger basalt aggregate size fraction is probably attributed to the following reasons: some aggregates with lower strength than paste, weaker interfacial transition zone (ITZ) between the aggregate and paste, and stress concentration at the contact points between those aggregates. Nevertheless, the decrease degree by basalt aggregate size effect is rather limited, which is similar to other researches [9]. It was even reported that the addition of coarse aggregate exhibits a slightly higher compressive strength [10]. In this case, the intrinsic strength of basalt aggregate is higher than ordinary aggregate, dense basalt can easily get a compressive strength more than 150 MPa. Besides, the ITZ between coarse basalt aggregate and paste can be stronger after optimization of powder content. Furthermore, with an appropriate powder content, the stress concentration can be improved by reducing contact points between the coarse aggregates. It can be concluded that it is possible to design UHPC with inclusion of coarse basalt aggregate.

3.3. Powder content effect

3.3.1. Compactness of UHPC

Packing density is defined as the ratio of the solid volume to bulk volume. Several models can be utilized to describe the packing density, such as Furnas Model, Toufar Model, Dewar Model, Linear Packing Density Model, Compressible Packing Model, etc. [66]. The Compressible Packing Model can present the compact-

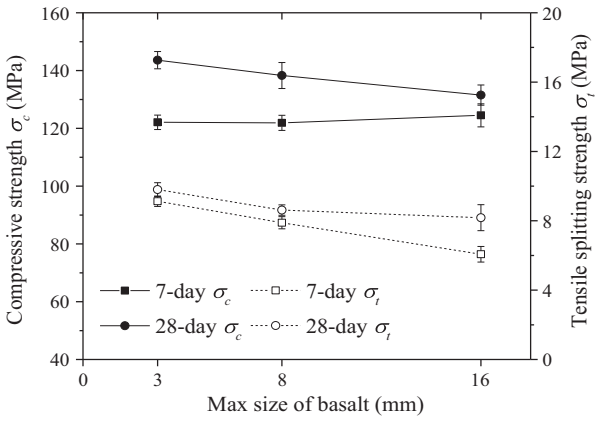

Fig. 10. Strength of UHPCs with different basalt sizes.

ness of a mixture via the virtual packing density β [67,68], calculated from:

$$\beta = min\left\{\frac{\beta_i}{1-\sum_{j=1}^{i-1}[1-\beta_i+b_{ij}\beta_i(1-1/\beta_j)]r_j-\sum_{j=i+1}^{n}(1-a_{ij}\beta_i/\beta_j)r_j}\right\} \quad (11)$$

$$\beta_j = (1+1/K)\alpha_j \quad (12)$$

$$a_{ij} = \sqrt{1-(1-d_j/d_i)^{1.02}} \quad (13)$$

$$b_{ij} = 1-(1-d_i/d_j)^{1.50} \quad (14)$$

in which a_{ij} and b_{ij} are interaction coefficients representing loosening effect and wall effect, respectively [67]; d_j is the average particle diameter of j-class particle and arranged in a sequence as $d_j > d_{j+1}$; β_j is the virtual packing density of the j-class particle; α_j is the experimentally determined packing density of j-class particle based on the EN 1097-3 [69]; K is the compaction index to determine the real packing density, the K value equal to 4.1 is used in this study, indicating no compaction is applied; r_j is the volume fraction of j-class particle.

The size class with the lowest β is called the dominant size class. In this study, the dominant grain is found always to be the cement grain based on the calculation by Eq. (11), where the packing density of individual ingredient is experimentally acquired. This also indicates that the cement consumes more space than the interstitials available between the large particles. Because the fractions of micro-silica and limestone powder are fixed based on the cement in this study, it can conclude that the powder content is the dominant factor which greatly influences the compactness of the designed UHPC. The packing densities of the designed UHPCs with basalt aggregate of 8 mm and 16 mm are shown in Fig. 11. In this study, a lower powder content contributes to a better compactness, which indicates a lower powder content is preferably used to design UHPC incorporating coarse aggregate.

3.3.2. Mechanical strength of UHPC

The above analysis shows great influence of powder content on the compactness of UHPC with coarse basalt aggregate. Hence, it is of great significance to investigate the powder content effect on the mechanical strength of UHPC. Fig. 12 shows the 28-day strength of UHPCs with different powder contents, using the maximum basalt size of 8 mm and 16 mm, respectively. Fig. 12(a) presents the strength of UHPCs with maximum basalt size of 8 mm. With the increase of powder content from 750 kg/m^3 to 900 kg/m^3, the compressive strength of UHPC first increases and then decreases, reaching the maximum value of 143 MPa at the powder content of 800 kg/m^3. The tensile splitting strength only has a slight fluctuation between 8.4 MPa and 9.1 MPa. Fig. 12(b) presents the strength of UHPCs with the maximum basalt size of 16 mm, which has a similar tendency to Fig. 12(a). The maximum compressive strength of 140 MPa occurs at the powder content of 700 kg/m^3, and the tensile splitting strength fluctuates between 6.5 MPa and 8.7 MPa.

The results indicate that the powder content effect has a greater influence on compressive strength rather than tensile strength of the designed UHPC. The optimal powder content occurs at a moderate value, rather than the highest content (900 kg/m^3) or the lowest content based on modified Andreasen and Andersen model. It indicates that the optimized mix design of UHPC with coarse basalt aggregate should incorporate an appropriate amount of powder to fill into the gaps between aggregate and avoid the possible stress concentration. The optimal powder content of UHPC is reducing from 800 kg/m^3 to 700 kg/m^3, with the maximum basalt size changing form 8 mm to 16 mm. It indicates that a lower powder dosage is requested to design UHPC when coarser aggregate is applied, which is in accordance with the results in Fig. 11.

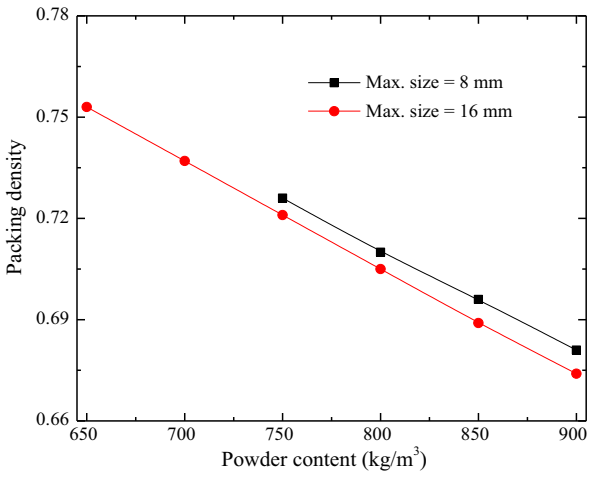

Fig. 11. Packing densities of UHPCs with different powder contents.

3.3.3. Distribution modulus q

The modified Andreasen and Andersen model has already been successfully employed in the optimization design for UHPC without coarse aggregate [39,40]. Different types of concrete can be designed using Eq. (1) by different values of distribution modulus q, which determines the proportion between fine and coarse particles. A smaller value of q contributes to a mixture rich in fine particles. Brouwers theoretically demonstrated the q value ranging of 0–0.28 [70], Hunger [39] and Yu [40] recommended using q in the range of 0.22–0.25 to design self-compacting concrete and UHPC with fine aggregate. However, an appropriate value of q has not been investigated for the UHPC incorporating coarse aggregate.

In this study, an initial q value of 0.22 is used to design UHPC with basalt aggregates. The PSD of the target and designed curves of UHPCs are shown in Fig. 13 (with the detailed mix proportion information in Table 3), according to Eqs. (1) and (2). Based on the modified Andreasen and Andersen model with q value of 0.22, the optimum powder contents can be computed, around 750 kg/m^3 and 650 kg/m^3 for the designed UHPC with basalt aggregate of 8 mm and 16 mm, respectively, as shown in Fig. 13. However, the maximum strengths occur at the powder contents of 800 kg/m^3 and 700 kg/m^3, respectively, which indicates that the chosen q value of 0.22 is slightly too high in this study. In order to get appropriate powder contents (800 kg/m^3 and 700 kg/mm^3) for excellent mechanical strength of UHPCs with coarse basalt aggregates, a lower distribution modulus q, is requested, yielding 0.19.

3.4. Interaction between coarse aggregate and steel fibre

Steel fibre is a critical parameter in designing UHPC because of its considerable reinforcement on mechanical properties. The strength of designed UHPFRCs, reinforced by 2 vol% steel fibre, are shown in Fig. 14.

The steel fibre reinforcement is researched on the UHPFRCs with different powder contents. Compared the results in Fig. 12 with those in Fig. 14, the powder content has a similar effect on mechanical strength, with and without 2% steel fibre. The optimum powder contents still occur at 800 kg/m^3 and 700 kg/m^3, respec-

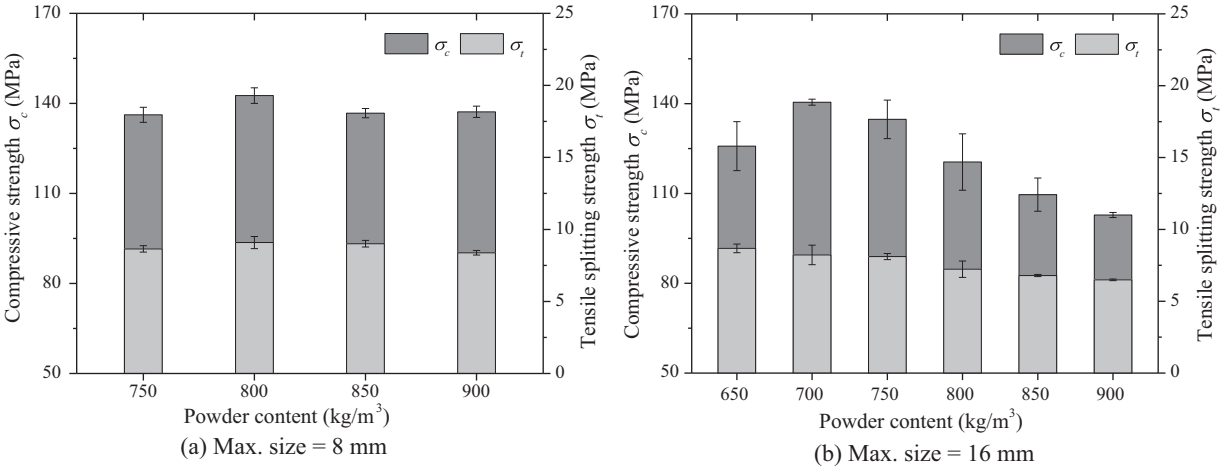

Fig. 12. Strength of UHPCs with different powder contents.

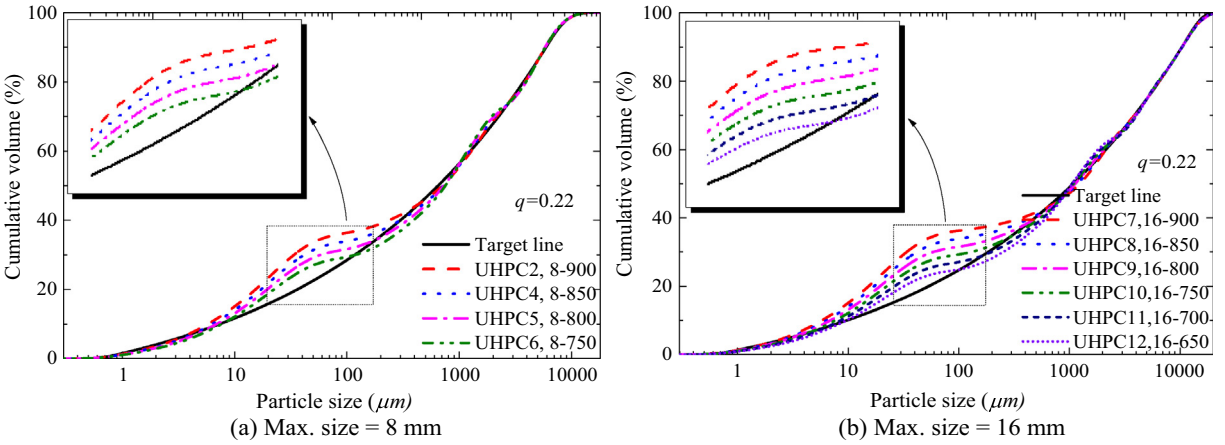

Fig. 13. PSDs of the target and designed curve of UHPCs.

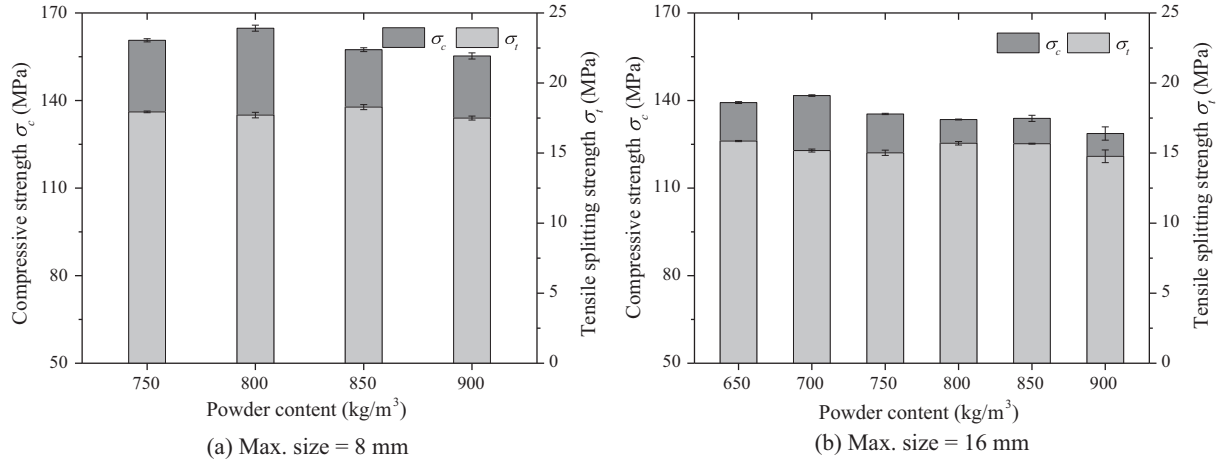

Fig. 14. Strength of UHPFRCs with different powder contents.

tively. The increase ratios of compressive strength of UHPCs are less than 25%. But, the increase ratios of tensile splitting strength are considerable, due to the bridging effect of steel fibre [71], between 83% and 131%. Fig. 15 shows the strength improvement ratios of UHPCs at a favourable powder content, 700 kg/m^3 and 800 kg/m^3. The strength improvement ratio of the mixture UHPC5 is always higher than that of the mixture UHPC11. A lower utilization efficiency of the 13 mm long steel fibre is observed for the UHPC containing coarser basalt aggregate, which indicates that the fibre-bridging stress interlock between fibre and coarse aggregate becomes worse. The steel fibre cannot completely overlay too large aggregate, subsequently the combined effect between steel

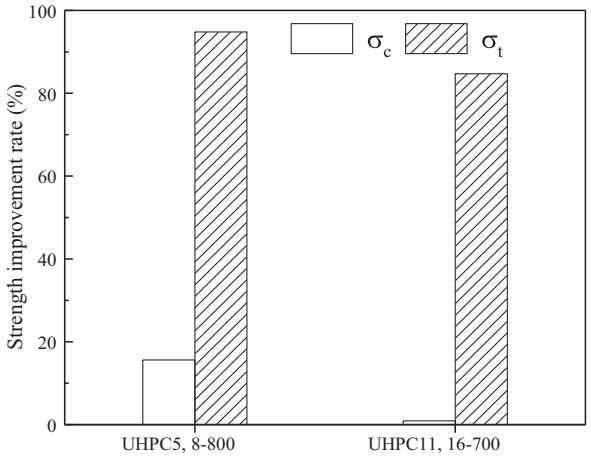

Fig. 15. Strength improvement rate by steel fibre.

fibre and bigger aggregate is weaker. Hence, steel fibre with proper length is suggested when designing UHPC with inclusion of relatively big aggregate.

4. Conclusions

This study investigates the effect of coarse aggregate size and the consequent alteration of powder content on the properties of UHPC. Moreover, the mineral admixture effect, and interaction between basalt aggregate and steel fibre are investigated. Based on the obtained results, the following conclusions can be drawn:

- The optimal proportion of powders is 5% of micro-silica and 20% of limestone powder by mass of the total powder, by considering the flowability, mechanical strength and shrinkage of UHPC pastes.
- Substitution of cement by 20% limestone powder results in enlarged shrinkage of UHPC paste up to 1.6 times after 91 days, attributed to the increasing capillary pores and free water amount. 5% micro-silica can greatly inhibit the shrinkage, with approximate 15% reduction.
- The coarse basalt aggregate results in a decrease on mechanical strength, but the decrease degree is rather limited. With the increase of particle size of basalt aggregate, both compressive and tensile splitting strengths tend to decrease, from 144 MPa to 132 MPa and 9.8 MPa to 8.2 MPa at 28 days, respectively.
- A reduced powder content is required to design UHPC when coarser aggregates are applied. The optimal powder content of UHPC in this study is about 800 kg/m^3 and 700 kg/m^3 with the maximum basalt aggregate of 8 mm and 16 mm, respectively. In addition, a distribution modulus q of 0.19 is recommended for the modified Andreasen and Andersen model.
- The optimal powder contents are the same for UHPCs without and with 2 vol% steel fibre. The reinforcement effect is more efficient on tensile strength rather than compressive strength, ranging from 83% and 131%. Fibres with appropriate lengths should be considered when designing UHPC with coarser aggregate.

Acknowledgements

This research was carried out under the funds of China Scholarship Council and Eindhoven University of Technology. Thanks are given to Mr. C.P. Chung for his help with experiments in this study. Furthermore, the authors wish to express their gratitude to ENCI for providing the used cement.

References

[1] P. Richard, M. Cheyrezy, Composition of reactive powder concretes, Cem. Concr. Res. 25 (1995) 1501–1511.
[2] D.Y. Yoo, N. Banthia, Mechanical properties of ultra-high-performance fiber-reinforced concrete: a review, Cem. Concr. Compos. 73 (2016) 267–280.
[3] R. Yu, L. van Beers, P. Spiesz, H.J.H. Brouwers, Impact resistance of a sustainable Ultra-high performance fibre reinforced concrete (UHPFRC) under pendulum impact loadings, Constr. Build. Mater. 107 (2016) 203–215.
[4] T. Makita, E. Brühwiler, Tensile fatigue behaviour of Ultra-High Performance fibre reinforced concrete combined with steel rebars (R-UHPFRC), Int. J. Fatigue. 59 (2014) 145–152.
[5] W. Wang, J. Liu, F. Agostini, C.A. Davy, F. Skoczylas, D. Corvez, Durability of an Ultra High performance fiber reinforced concrete (UHPFRC) under progressive aging, Cem. Concr. Res. 55 (2014) 1–13.
[6] C. Shi, Z. Wu, J. Xiao, D. Wang, Z. Huang, Z. Fang, A review on ultra high performance concrete: part I. Raw materials and mixture design, Constr. Build. Mater. 96 (2015) 368–377.
[7] K. Rozalija, D. Darwin, Effects of Aggregate Type, Size, and Content on Concrete Strength and Fracture Energy, Lawrence, Kansas, 1997.
[8] J. Ma, M. Orgass, F. Dehn, D. Schmidt, N. V. Tue, Comparative Investigations on Ultra-High Performance Concrete with or without Coarse Aggregates, Proc. Int. Symp. Ultra High Perform. Concr. Kassel. (2004) 205–212.
[9] S. Collepardi, L. Coppola, R. Troli, M. Collepardi, Mechanical properties of modified reactive powder concrete, ACI Spec. Publ. 173 (1997) 1–22.
[10] K. Wille, A.E. Naman, G.J. Parra-Montesinos, Ultra-High Performance Concrete with compressive strength exceeding 150 MPa (22ksi): A Simpler Way, ACI Mater. J. 108 (2011) 46–53.
[11] Y. Peng, H. Wu, Q. Fang, J.Z. Liu, Z.M. Gong, Impact resistance of basalt aggregated UHP-SFRC/fabric composite panel against small caliber arm, Int. J. Impact Eng. 88 (2016) 201–213.
[12] Y.S. Tai, S. El-Tawil, T.H. Chung, Performance of deformed steel fibers embedded in ultra-high performance concrete subjected to various pullout rates, Cem. Concr. Res. 89 (2016) 1–13.
[13] R. Yu, P. Spiesz, H.J.H. Brouwers, Effect of nano-silica on the hydration and microstructure development of Ultra-High Performance Concrete (UHPC) with a low binder amount, Constr. Build. Mater. 65 (2014) 140–150.
[14] B. Vermeulen, Ultra High Performance Concrete in Action, 2nd Grad. Lab AE Conf. 2013.
[15] I.M. Nikbin, M.H.A. Beygi, M.T. Kazemi, J. Vaseghi Amiri, S. Rabbanifar, E. Rahmani, S. Rahimi, A comprehensive investigation into the effect of water to cement ratio and powder content on mechanical properties of self-compacting concrete, Constr. Build. Mater. 57 (2014) 69–80.
[16] P.L. Domone, A review of the hardened mechanical properties of self-compacting concrete, Cem. Concr. Compos. 29 (2007) 1–12.
[17] D.P. Bentz, P.E. Stutzman, Evolution of porosity and calcium hydroxide in laboratory concretes containing silica fume, Cem. Concr. Res. 24 (1994) 1044–1050.
[18] P. Duan, Z. Shui, W. Chen, C. Shen, Effects of metakaolin, silica fume and slag on pore structure, interfacial transition zone and compressive strength of concrete, Constr. Build. Mater. 44 (2013) 1–6.
[19] C. Shi, D. Wang, L. Wu, Z. Wu, The hydration and microstructure of ultra high-strength concrete with cement–silica fume–slag binder, Cem. Concr. Compos. 61 (2015) 44–52.
[20] M. Nili, A. Ehsani, Investigating the effect of the cement paste and transition zone on strength development of concrete containing nanosilica and silica fume, Mater. Des. 75 (2015) 174–183.
[21] D.P. Bentz, C.F. Ferraris, S.Z. Jones, D. Lootens, F. Zunino, Limestone and silica powder replacements for cement: early-age performance, Cem. Concr. Compos. 78 (2017) 43–56.
[22] G. Kakali, S. Tsivilis, E. Aggeli, M. Bati, Hydration products of C3A, C3S and Portland cement in the presence of CaCO3, Cem. Concr. Res. 30 (2000) 1073–1077.
[23] M. Nehdi, S. Mindess, P.C. Aïtcin, Optimization of high strength limestone filler cement mortars, Cem. Concr. Res. 26 (1996) 883–893.
[24] W. Zhu, J.C. Gibbs, Use of different limestone and chalk powders in self-compacting concrete, Cem. Concr. Res. 35 (2005) 1457–1462.
[25] Z. Wu, C. Shi, K.H. Khayat, Influence of silica fume content on microstructure development and bond to steel fiber in ultra-high strength cement-based materials (UHSC), Cem. Concr. Compos. 71 (2016) 97–109.
[26] D.Y. Lei, L.P. Guo, W. Sun, J. Liu, X. Shu, X.L. Guo, A new dispersing method on silica fume and its influence on the performance of cement-based materials, Constr. Build. Mater. 115 (2016) 716–726.
[27] J. Yajun, J.H. Cahyadi, Effects of densified silica fume on microstructure and compressive strength of blended cement pastes, Cem. Concr. Res. 33 (2003) 1543–1548.
[28] L. Soufeiani, S.N. Raman, M.Z. Bin Jumaat, U.J. Alengaram, G. Ghadyani, P. Mendis, Influences of the volume fraction and shape of steel fibers on fiber-reinforced concrete subjected to dynamic loading – A review, Eng. Struct. 124 (2016) 405–417.
[29] K. Habel, M. Viviani, E. Denarié, E. Brühwiler, Development of the mechanical properties of an Ultra-High Performance Fiber Reinforced Concrete (UHPFRC), Cem. Concr. Res. 36 (2006) 1362–1370.
[30] G.H. Mahmud, Z. Yang, A.M.T. Hassan, Experimental and Numerical Studies of Size effects of Ultra High Performance Steel Fibre Reinforced Concrete (UHPFRC) beams, Constr. Build. Mater. 48 (2013) 1027–1034.

[31] W. Meng, M. Valipour, K.H. Khayat, Optimization and performance of cost-effective ultra-high performance concrete, Mater. Struct. 50 (2017) 29.
[32] M. Alkaysi, S. El-Tawil, Z. Liu, W. Hansen, Effects of silica powder and cement type on durability of ultra high performance concrete (UHPC), Cem. Concr. Compos. 66 (2016) 47–56.
[33] C.P. Gu, G. Ye, W. Sun, Ultrahigh performance concrete-properties, applications and perspectives, Sci. China Technol. Sci. 58 (2015) 587–599.
[34] J.E. Funk, D.R. Dinger, Predictive Process Control of Crowded Particulate Suspensions: Applied to Ceramic Manufacturing, Kluwer Academic Publishers, 1994.
[35] H.J.H. Brouwers, H.J. Radix, Self-compacting concrete: Theoretical and experimental study, Cem. Concr. Res. 35 (2005) 2116–2136.
[36] G. Quercia, G. Hüsken, H.J.H. Brouwers, Water demand of amorphous nano silica and its impact on the workability of cement paste, Cem. Concr. Res. 42 (2012) 344–357.
[37] Q.L. Yu, P. Spiesz, H.J.H. Brouwers, Development of cement-based lightweight composites – Part 1: mix design methodology and hardened properties, Cem. Concr. Compos. 44 (2013) 17–29.
[38] Q.L. Yu, H.J.H. Brouwers, Development of a self-compacting gypsum-based lightweight composite, Cem. Concr. Compos. 34 (2012) 1033–1043.
[39] M. Hunger, An integral design concept for ecological self-compacting concrete, PhD thesis, Eindhoven Universtiy of Technology, Eindhoven, the Netherland, 2010.
[40] R. Yu, Development of sustainable protective Ultra-High Performance Fibre Reinforced Concrete (UHPFRC), PhD thesis, Eindhoven Universtiy of Technology, Eindhoven, the Netherland, 2015.
[41] EN-1015-3, Methods of test for mortar for masonry – Part 3: Determination of consistence of fresh mortar (by flow table), Br. Stand. Institution-BSI CEN Eur. Comm. Stand. (2007).
[42] Q.L. Yu, H.J.H. Brouwers, Microstructure and mechanical properties of β-hemihydrate produced gypsum: an insight from its hydration process, Constr. Build. Mater. 25 (2011) 3149–3157.
[43] P.P. Li, Q.L. Yu, H.J.H. Brouwers, Effect of PCE-type superplasticizer on early-age behaviour of ultra-high performance concrete (UHPC), Constr. Build. Mater. 153 (2017) 740–750.
[44] EN 12390-3, Testing hardened concrete – Part 3: Compressive strength of test specimens, Br Stand. Institution-BSI CEN Eur. Comm. Stand., 2009.
[45] EN-196-1, Methods of testing cement – Part 1: Determination of strength., Br. Stand. Institution-BSI CEN Eur. Comm. Stand. (2005).
[46] EN 12390-6, Testing hardened concrete – Part 6: Tensile splitting strength of test specimens, Br Stand. Institution-BSI CEN Eur. Comm. Stand., 2000.
[47] DIN 52-450, Determination of Shrinkage and Expansion of small test specimens, Ger. Stand. (1985).
[48] M. Hajime Okamura, Ouchi, self-compacting concrete, J. Adv. Concr. Technol. 1 (2003) 5–15.
[49] P. Domone, C. Hsi-wen, Testing of binders for high performance concrete, Cem. Concr. Res. 27 (1997) 1141–1147.
[50] C. Schröfl, M. Gruber, J. Plank, Preferential adsorption of polycarboxylate superplasticizers on cement and silica fume in ultra-high performance concrete (UHPC), Cem. Concr. Res. 42 (2012) 1401–1408.
[51] W. Sekkal, A. Zaoui, Nanoscale analysis of the morphology and surface stability of calcium carbonate polymorphs, Sci. Rep. 3 (2013) 1587.
[52] P. Hosseini, A. Booshehrian, A. Madari, Developing concrete recycling strategies by utilization of nano-SiO 2 particles, Waste Biomass Valorization. 2 (2011) 347–355.
[53] A. Itim, K. Ezziane, E.H. Kadri, Compressive strength and shrinkage of mortar containing various amounts of mineral additions, Constr. Build. Mater. 25 (2011) 3603–3609.
[54] K. Vance, M. Aguayo, T. Oey, G. Sant, N. Neithalath, Hydration and strength development in ternary portland cement blends containing limestone and fly ash or metakaolin, Cem. Concr. Compos. 39 (2013) 93–103.
[55] C. Wang, C. Yang, F. Liu, C. Wan, X. Pu, Preparation of Ultra-High Performance Concrete with common technology and materials, Cem. Concr. Compos. 34 (2012) 538–544.
[56] K. Mermerdaş, M.M. Arbili, Explicit formulation of drying and autogenous shrinkage of concretes with binary and ternary blends of silica fume and fly ash, Constr. Build. Mater. 94 (2015) 371–379.
[57] W. Zhang, Y. Hama, S.H. Na, Drying shrinkage and microstructure characteristics of mortar incorporating ground granulated blast furnace slag and shrinkage reducing admixture, Constr. Build. Mater. 93 (2015) 267–277.
[58] C. Varhen, I. Dilonardo, R.C. de Oliveira Romano, R.G. Pileggi, A.D. de Figueiredo, Effect of the substitution of cement by limestone filler on the rheological behaviour and shrinkage of microconcretes, Constr. Build. Mater. 125 (2016) 375–386.
[59] R. Detwiler, P.D. Tennis, The Use of Limestone in Portland Cement : A State-of-the-Art Review, 2003.
[60] P.D. Tennis, M.D.A. Thomas, W.J. Weiss, State-of-the-art report on use of limestone in cements at levels of up to 15%, Portl. Cem. Assoc. (2011) 1–78.
[61] J.K. Mackenzie, The elastic constants of a solid containing spherical holes, Proc. Phys. Soc. Sect. B 63 (2002) 2–11.
[62] D.P. Bentz, A review of early-age properties of cement-based materials, Cem. Concr. Res. 38 (2008) 196–204.
[63] W. Wongkeo, P. Thongsanitgarn, A. Chaipanich, Compressive strength and drying shrinkage of fly ash-bottom ash-silica fume multi-blended cement mortars, Mater. Des. 36 (2012) 655–662.
[64] Y. Benachour, C.A. Davy, F. Skoczylas, H. Houari, Effect of a high calcite filler addition upon microstructural, mechanical, shrinkage and transport properties of a mortar, Cem. Concr. Res. 38 (2008) 727–736.
[65] S.H. Alsayed, Influence of superplasticizer, plasticizer, and silica fume on the drying shrinkage of high-strength concrete subjected to hot-dry field conditions, Cem. Concr. Res. 28 (1998) 1405–1415.
[66] S.A.A.M. Fennis, Design of Ecological Concrete by Particle Packing Optimization PhD thesis, Delft University of Technology, Delft, the Netherlands, 2009.
[67] C.F. Ferraris, F. de Larrard, Testing and Modelling of Fresh Concrete Rheology, NISTIR 6094, Maryland, United States, 1998.
[68] J. Van Der Putten, J. Dils, P. Minne, V. Boel, G. De Schutter, Determination of packing profiles for the verification of the compressible packing model in case of UHPC pastes, Mater. Struct. 50 (2017) 118.
[69] EN-1097-3, Tests for mechanical and physical properties of aggregates- Part 3: Determination of loose bulk density and voids, Br. Stand. Institution-BSI CEN Eur. Comm. Stand. (1998).
[70] H.J.H. Brouwers, Particle-size distribution and packing fraction of geometric random packings, Phys. Rev. E 74 (2006) 31309.
[71] R. Madandoust, M.M. Ranjbar, R. Ghavidel, S. Fatemeh, Shahabi, assessment of factors influencing mechanical properties of steel fiber reinforced self-compacting concrete, Mater. Des. 83 (2015) 284–294.